

Nanorod-structured Fe₃O₄/Graphene Nanocomposite as High Performance Anode for Lithium-Ion Batteries

Yanglin Liu^{1,2}, Yaping Wang¹, Anqiang Pan^{1,*}

¹ School of Materials Science and Engineering, Central South University, Changsha, Hunan 410083, China

² Changsha Environmental Protection Vocational College, Changsha 410004, Hunan, China

*E-mail: pananqiang@csu.edu.cn

Received: 24 October 2016 / Accepted: 19 January 2017 / Published: 12 February 2017

High capacity Fe₃O₄ nanorod/graphene composites with good rate capability were prepared by a two-step synthesis process: FeOOH/graphene composites were first synthesized by uniformly dispersed, hydrothermal prepared FeOOH nanorods on functionalized graphene sheets, and then they were annealed in an argon atmosphere at 450°C for 2 h to make Fe₃O₄/graphene composites. The graphene functions as a reducing reagent during the annealing process. Thus synthesized Fe₃O₄ nanorods with small diameters ranging from 50 nm to 100 nm have an intimate electrical contact with graphene sheet and exhibit excellent electrochemical properties. The Fe₃O₄ nanorod/graphene nanocomposite shows a superior high reversible specific capacity (1155 mAh g⁻¹) and good rate capability, demonstrating it is a promising alternative electrode material for high-performance lithium-ion batteries.

Keywords: graphene; Fe₃O₄ nanorod; anode; lithium-ion batteries; high rate

1. INTRODUCTION

High energy storage systems are needed to reduce our reliance on fossil fuels and minimize environmental pollution associated with the use of fossil fuels [1]. Because of the high energy density, long cycle life and flexible design, lithium-ion batteries have been the predominant power sources for high-end consumer electronic devices such as cell phones, laptop computers, and more recently hybrid and electrical vehicles. However, the need for higher energy and power continue increases with rapidly increasing demand such as long rang electrical vehicles. The conventional graphite anode currently used in commercial lithium-ion batteries possesses a limited specific capacity (< 370 mAh/g). Various materials—graphitic/non-graphitic carbons [2], alloying materials with lithium (silicon, tin, Sb) [3-6], transition-metal oxides [7-10], and nitrides [11]—have been studied as alternate anode materials for

lithium-ion batteries because of their higher capacities. Recently, the inverse spinel-structured Fe_3O_4 has attracted much attention because it can react with more lithium ions through conversion reactions to give a much higher reversible theoretical specific capacity (924 mAh/g) [12-14], which is more than two times larger than that of graphite (372 mAh/g) [15]. At room temperature, the inverse spinel exhibits an electronic conductivity as high as 2×10^{-4} S/m [16]. Furthermore, Fe_3O_4 is environmentally benign and naturally abundant. However, upon charge/discharge cycling, Fe_3O_4 suffers large volume expansions, contractions and structural degradation, which leads to severe irreversible capacity losses during cycling [12, 14, 16]. Although it has been demonstrated that the cycling stability and the reversible capacity of Fe_3O_4 can be improved by reducing the particle size to the nanoscale, it is still a significant challenge to achieve highly reversible capacity, long cycle, and rate capability [16-18]. Recently, a new Fe_3O_4 /SWNT (single-walled carbon nanotube) nanocomposite was developed, using the SWNTs as the thermal and electronic conductive phase. This material achieved a high-rate capacity and stability. Since SWNTs are still expensive to produce, new nanoscale carbon materials will be desirable to achieve similar performance.

Graphene, which is a new, two-dimensional, exfoliated graphite material, has superior electrical conductivity, high surface area, ultrathin thickness, and structural flexibility [19-23]. Recently, it also was discovered that a graphene sheet has a large reversible capacity (~ 500 mAh/g) when used as the anode in lithium batteries [24-26]; however, it suffers from large capacity fading during the initial cycles. Another interesting application would be to use graphene to improve the conductivity and structural integrity in a nanocomposite for energy storage. Various synthesized composites of graphene and active nano-materials have been found to possess superior performance characteristics [27-30]. In these composites, graphene serves as a good conductor for electron transport, while effectively accommodates the volume changes in active materials and prevents aggregation of the nanoparticles. Meanwhile, the nanoparticles located between the graphene nanosheets can effectively reduce the degree of graphene restacking, consequently maintaining their high active surface area. All of these factors contribute to a higher lithium storage capacity and improved cyclic performance [28-29, 31]. Therefore, the good conductivity, mechanical strength and flexibility of graphene make it an excellent alternative component for Fe_3O_4 composite materials. Very recently, a Fe_3O_4 /graphene composite with a particle size around 200 nm was reported by in-situ anchoring FeOOH on graphene sheet, then through self-reducing to produce Fe_3O_4 /graphene composite at elevated temperature [32]. Although these in situ formed Fe_3O_4 /graphene composites exhibit good cycle stability, reversible capacity and rate capability, their performance is much lower than those reported for the SWNT system, in which a two-step synthesis process are employed.

In this work, we adapted a two-step synthesis process (similar to those used in the synthesis of Fe_3O_4 /SWNT composite) to fabricate Fe_3O_4 /graphene composite. The structure of the composite was characterized and the electrochemical performance, such as high reversible capacity and good rate capabilities are reported. The results demonstrate that the two-step synthesis approach reported here is an effective way to obtain high performance electrode for lithium ion batteries.

2. EXPERIMENTAL SECTIONS

FeOOH nanorods as the precursor for Fe₃O₄ nanorods were prepared using a hydrothermal process similar to the method reported in the literature [33]. FeCl₃ (0.405 g) was dissolved in 20 mL of distilled water, and then was added to a 20-mL NaOH (0.400 g) solution. The mixture was stirred to form a homogeneous red gel before it was transferred to a 40-mL, Teflon-lined, stainless-steel autoclave. The reaction was maintained at 140°C for 12 hours. After cooling to room temperature, the yellow-colored FeOOH nanorods precipitation was obtained by filtration for further use. One gram of SDS was dissolved in distilled water, and 100 mg of graphene sheets (Vorbeck Materials (Jessup, Maryland)) was added to the SDS solution; this mixture underwent ultrasonic treatment (i.e., sonication) for 30 minutes to form functionalized graphene sheets (referred as graphene in this paper). Pre-synthesized FeOOH nanorods from the hydrothermal process were poured into the graphene-water suspension and actively stirred for 30 minutes. The mixture was then sonicated for 30 minutes before undergoing separation by vacuum filtration. The whole process was repeated several times to remove the extra SDS in the solution. The resulting film was dried under vacuum at 80°C over night and then baked in an argon atmosphere at 450°C for 2 hours. For the x-ray diffraction (XRD) experiment, FeOOH precursor samples also were washed with distilled water and dried under vacuum, followed by baking in an argon atmosphere at 450°C for 2 hour.

The crystalline structure of the as-prepared FeOOH, its annealed product, and Fe₃O₄/graphene nanocomposite were determined by XRD analysis using a Scintag XDS2000 θ - θ powder diffractometer equipped with a germanium (lithium) solid-state detector and a copper K α sealed tube ($\lambda=1.54178$ Å). The samples were scanned in the range between 10° and 70° (2 θ), with a step size of 0.02° and an exposure time of 10 seconds. Scanning electron microscopy (SEM) (FEI Helios 600 Nanolab FIB-SEM, 3 KV) was used to characterize the particle morphology. Transmission electron microscopy (TEM) analysis was carried out on a Jeol JEM 2010 microscope fitted with a LaB₆ filament and an acceleration voltage of 200 kV. A combined differential scanning calorimetry/thermal gravimetric analysis (DSC/TGA) instrument (Mettler-Toledo, TGA/DSC STAR system) was used to study the content of graphene in the nanocomposites by increasing the temperature from room temperature to 600°C in air. The flow rate of air was 50 cm³ min⁻¹ and the temperature ramp rate was 10°C min⁻¹. Nitrogen adsorption-desorption measurements were conducted at 77K (NOVA 4200e, Quantachrome Instruments). The Fe₃O₄/graphene composite was degassed at 50°C for 18 hours before adsorption and desorption measurements.

Raman measurements were performed using an argon-ion laser with 514.5 nm wavelength excitation. A 20-mW laser was used for this Raman measurement, and no thermal effects were observed on the samples throughout the measurements. The laser beam was chopped by a mechanical shutter to control the exposure time. Each Raman spectrum was obtained by accumulating 10 measurements, with the exposure time for each measurement being 20 seconds. A spectrometer (Princeton Instruments, Spectrapro 2500i) with a back illuminated charge-coupled detector attachment (Princeton Instruments, Spec 10) was used to obtain Raman spectra.

To make into the electrode, Fe₃O₄/graphene material was mixed with poly(vinylidene fluoride) (PVDF) binder (at a weight ratio of 9:1) in *N*-methyl-2-pyrrolidone (NMP) to make a slurry, which

was spread onto a copper foil and dried in a vacuum oven at 100°C overnight. For comparison, a graphene sheet was made into the electrode using the same process and a graphene-to-PVDF ratio of 9:1 by weight. A micro-sized Fe₃O₄/Super P/PVDF electrode also was made by mixing commercially obtained micro-sized Fe₃O₄ powders, Super P carbon, and PVDF at weight ratios of 8:1:1, respectively.

Electrodes were tested in coin-cells (2325 coin cell, National Research Council, Canada) assembled in a glove box (MBraun, Inc.) filled with ultra-high-purity argon. The cells used polypropylene membrane (Celgard 3501) as the separator, lithium metal as the anode, and 1-M LiPF₆ in ethyl carbonate/dimethyl carbonate (1:1 v/v) as the electrolyte. The electrochemical performances of the electrodes were evaluated on an Arbin Battery Tester BT-2000 (Arbin Instruments) at room temperature. The Fe₃O₄/graphene nanocomposite cells were tested in a voltage range of 0.01~3 V vs. Li/Li⁺ at various charging rates, in which the mass was based on the whole weight of Fe₃O₄/graphene composite. For graphene and micro-sized Fe₃O₄ samples, the capacity was based on the weights of the graphene and the Fe₃O₄, respectively. Cyclic voltammograms (CVs) were developed for three electrode configurations, in which lithium foil served as both the counter and reference electrodes and the Fe₃O₄/graphene nanocomposite was used as the working electrode.

3. RESULTS

3.1. Structural Characterization

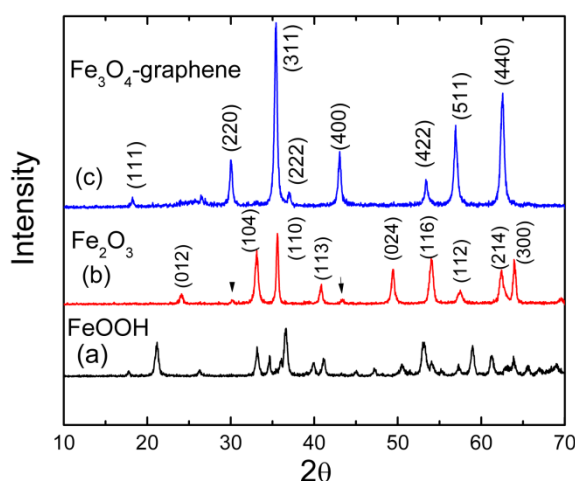


Figure 1. XRD patterns for the hydrothermal product: (a) FeOOH, (b) the annealed product of FeOOH under an argon atmosphere at 450°C for 2 hours, and (c) the nanostructured Fe₃O₄/graphene composite prepared by annealing FeOOH and graphene composite in an argon atmosphere at 450°C for 2 hours.

The XRD patterns of the prepared materials are shown in Figure 1. The hydrothermal product before annealing (Figure 1a) has all the peaks belonging to the tetragonal α -FeOOH phase (goethite, JCPDS 81-0463). After annealing in an argon atmosphere at 450°C for 2 hour, the material (Figure 1b) shows XRD patterns of the Fe₂O₃ phase (JCPDS 33-0664), except for two weak peaks associated with

Fe_3O_4 phase (JCPDS 88-0315) as indicated by the arrow sites. Figure 1c shows the XRD pattern of the annealed product of Fe_3O_4 nanorods with the graphene composite material. All the peaks are indexed and can be attributed to the Fe_3O_4 phase (JCPDS 88-0315), which suggests the successful fabrication of Fe_3O_4 /graphene composite. It is worth noting that the valence of irons changed from Fe^{3+} (FeOOH) to mixed valences of $\text{Fe}^{3+/2+}$ (Fe_3O_4). Considering the fact that the carbon-to-oxygen ratio of the graphene material used in this work is approximately 14 [34], the oxygen released during the reduction of Fe^{3+} may react with the graphene sheet and lead to a decreased carbon-to-oxygen ratio. This interaction will form a stable binding between Fe_3O_4 and graphene nanosheets and lead to a highly reversible structure as discussed below. There is only one weak peak related to the graphite phase even at 450°C , which suggests stacking of graphene sheets into several layers is limited probably because of the good dispersion of the FeOOH nanorods within the graphene matrix.

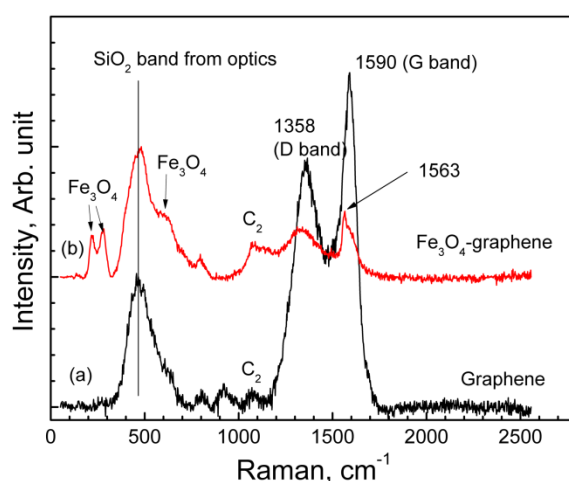


Figure 2. Raman results of pristine graphene (a) and Fe_3O_4 /graphene nanocomposite (b).

Figure 2 shows the Raman experiment results of pristine functionalized graphene sheets (a) and the Fe_3O_4 /graphene composite (b). The observed D band (1358 cm^{-1}) and G band (1590 cm^{-1}) are the typical bands for graphene materials. As for the nanocomposite, some extra peaks belonging to Fe_3O_4 phase also were detected, which are consistent with the formation of Fe_3O_4 /graphene composite. However, when compared to the spectrum of pristine graphene, red shifts for the D and G bands (towards to smaller wave number) were observed, which might be attributed to the interaction between Fe_3O_4 and graphene sheets. The peaks around 1000 cm^{-1} of pristine graphene sheets correspond well with the calculated Raman spectra of graphene with a C_2 vacancy (relaxed 5-8-5 defect structure) [35]. The relative intensity of $I_{\text{C}_2}/I_{\text{G}}$ becomes larger for the nanocomposite material when compared to that of the graphene sheets, which indicates that the vacancy increase for the graphene sheet in the Fe_3O_4 /graphene composite materials. The increased vacancy is related to the reduction of FeOOH precursor during the annealing process.

TG analysis and DTA were used to determine the content of graphene in the as-synthesized Fe_3O_4 /graphene composite, and the results are shown in Figure 3. The slight weight change shown on the TG curve and a broad peak on the DTA curve at temperatures below 400°C are attributed to the slow oxidation of graphene in air and partial oxidation of Fe_3O_4 to Fe_2O_3 . However, the major drop

shown on the TG curve and the large exothermal peak shown on the DTA curve at a temperature larger than 400°C indicate a significant mass loss from graphene. The typical color of the final product was red, suggesting that the Fe_3O_4 was totally oxidized to Fe_2O_3 . According to the TG and DTA results, the amount of graphene in the composite was about 40 percent.

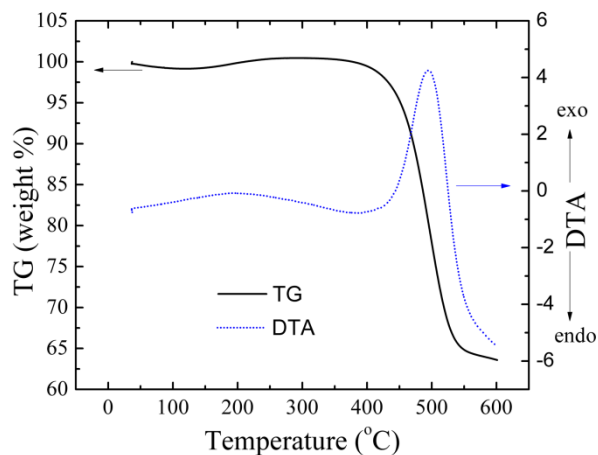


Figure 3. TG and DTA curves of Fe_3O_4 /graphene nanocomposite. The air flow rate was $50 \text{ cm}^3 \text{ min}^{-1}$, and the temperature ramp rate was $10^\circ\text{C}/\text{min}$.

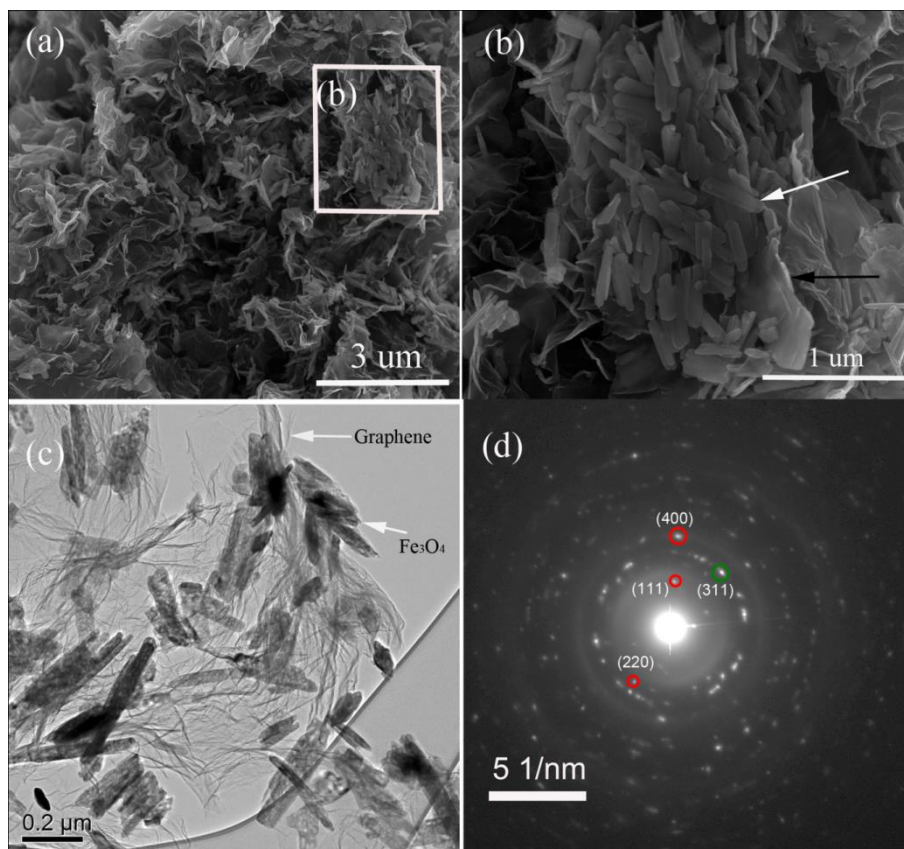


Figure 4. Structural characterization of the Fe_3O_4 /graphene composite: SEM images obtained at low magnification (a), SEM images obtained at high magnification (b) (the white arrow indicates the Fe_3O_4 nanorod, and the black arrow indicates the graphene sheets), TEM image (c), and the corresponding diffraction pattern (d).

Figure 4 shows the morphologies and structure of the as-synthesized $\text{Fe}_3\text{O}_4/\text{graphene}$ nanocomposites. As shown in Figure 4a, the Fe_3O_4 nanorods are well dispersed in the graphene matrix. Figure 4b is a high magnification SEM image of the nanocomposite. As indicated by the white arrow, the morphology of the Fe_3O_4 nanorods is quite uniform, and the attachment of the particles with the graphene sheets is good, as indicated by the black arrow. As shown in the TEM image (Figure 4c) of the nanocomposite, the nanorods are uniformly distributed on the graphene sheets, and the diameters of the nanorods are in the range of 50 nm to 100 nm. The good attachment of the nanorod on the graphene sheets allows rapid electron transport through the underlying graphene layers. Furthermore, the graphene sheets effectively limit the aggregation of the Fe_3O_4 during the electrochemical cycling process. On the other hand, the nanorod particles on the graphene sheets can act as spacers to effectively prevent the close restacking of graphene sheets, thus avoiding or reducing the loss of their high active surface area. The TEM diffraction pattern in Figure 4d shows the crystalline structure of the Fe_3O_4 nanorods. The diffraction rings can be indexed to the cubic $Fd\bar{3}m$ crystal structure [12].

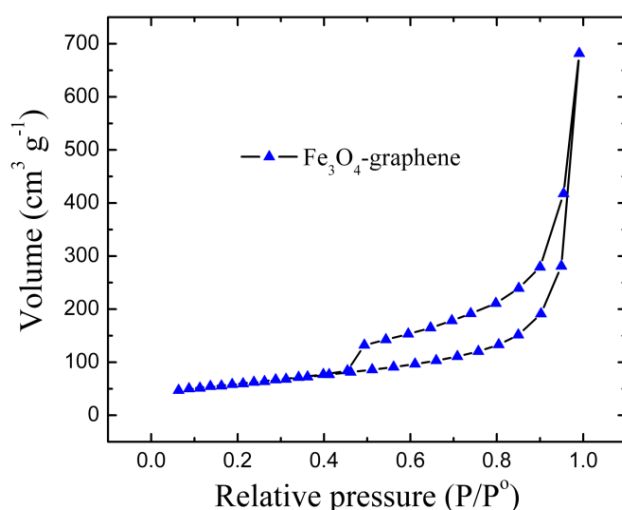


Figure 5. Nitrogen sorption isotherms measured at 77K of the $\text{Fe}_3\text{O}_4/\text{graphene}$ nanocomposite.

Figure 5 shows the typical nitrogen sorption isotherms of the as-synthesized $\text{Fe}_3\text{O}_4/\text{graphene}$ composite. The isotherm of the nanocomposite shows a typical IV-type curve with a clear H1-type hysteric loop [36-37], which is characteristic of mesoporous materials. The Brunauer-Emmett-Teller surface area of the sample was measured as $206 \text{ m}^2/\text{g}$, which is much larger than those reported recently by Zhou et al. [32] for micro-sized Fe_3O_4 ($2 \text{ m}^2/\text{g}$) and graphene/ Fe_3O_4 nanocomposite ($53 \text{ m}^2/\text{g}$), thus it facilitates better electrolyte penetration in our nanocomposite. The pore volume of $1.11 \text{ cm}^3/\text{g}$ in our material also is higher than the pore volume reported in the literature (i.e., $0.23 \text{ cm}^3/\text{g}$). The porous structures of macropores and mesopores may facilitate electrolyte diffusion to active sites with less resistance [38] and provide better tolerance to the volume changes [39] of Fe_3O_4 particles during charge/discharge processes.

3.2. Electrochemical Performance

The electrochemical performance of the nanorod Fe_3O_4 /graphene composite was evaluated by galvanostatic charge/discharge cycling at a current density of 100 mA/g, and the results are illustrated in Figure 6.

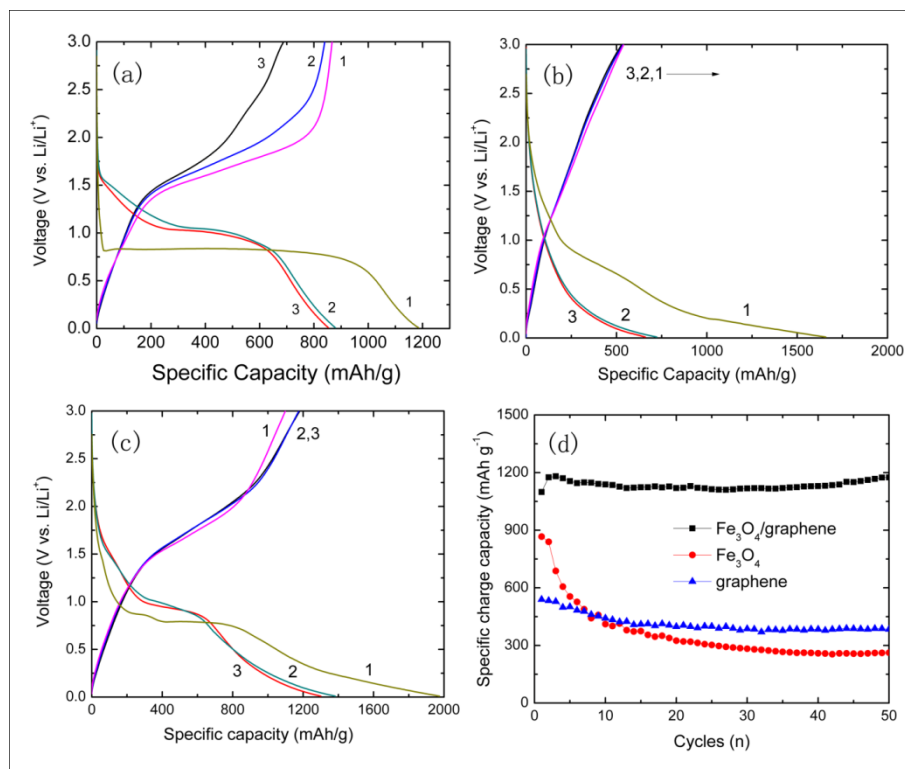


Figure 6. Discharge/charge curves of the first three cycles for the micro-sized Fe_3O_4 electrode (a), the graphene (b), and the Fe_3O_4 /graphene nanocomposite (c), and their cycling performances (d).

For comparison, the results of pure micro-sized Fe_3O_4 (Figures 6a and 6d) and graphene (Figures 6b and 6d) tested under the same electrochemical conditions also are presented. Figures 6a, 6b, and 6c show the charge/discharge profiles for the first three cycles for the micro-sized Fe_3O_4 , graphene and Fe_3O_4 /graphene nanocomposite, respectively. In the first discharge step, the Fe_3O_4 /graphene nanocomposite reaches a plateau at about 0.75 V, which is typical for Fe_3O_4 electrodes, and then decreases to the cutoff voltage of 0.01 V, which is more typical for graphene electrode. The first discharge and charge capacities are 1970 mAh/g and 1098 mAh/g for the Fe_3O_4 /graphene nanocomposite, 1184 mAh/g and 866 mAh/g for the micro-sized Fe_3O_4 , and 1670 mAh/g and 539 mAh/g for the graphene electrode. The initial capacity loss may result from the incomplete conversion reaction and the irreversible lithium loss due to the formation of a solid electrolyte interface layer [33, 40]. As shown in Figure 6a, the reversible capacity of the micro-sized Fe_3O_4 electrode decreases rapidly, mainly because of its limited ability to accommodate volume changes during cycling. The reversible capacity of the graphene electrode also decreases significantly during the first few cycles (as shown in Figure 6b). However, the reversible capacity of Fe_3O_4 /graphene nanocomposite electrode increases slightly from 1098 mAh/g to 1180 mAh/g and remains stable as indicated by the negligible

charge capacity difference (shown in Figure 6c). The cycling performances of the three electrodes are compared in Figure 6d. Within 50 cycles, the charge capacities of graphene and Fe₃O₄-microparticles electrodes decrease from 639 mAh/g to about 484 mAh/g and from 866 mAh/g to 262 mAh/g, respectively. In contrast, the reversible capacity of the Fe₃O₄/graphene nanocomposite increases slightly during the initial cycles and becomes quite stable at the fifth cycle with a specific charge capacity of 1155 mAh/g, which is much higher than the reversible capacity of graphene and micro-sized Fe₃O₄ electrodes. The reversible capacity of the Fe₃O₄/graphene nanocomposite is higher than the theoretical capacity of Fe₃O₄ (924 mAh/g). The extra discharge capacity of the Fe₃O₄/graphene nanocomposite might be attributed to 1) the surface adsorption/desorption of lithium ions because of the large surface area of the composite (206 m²/g) and 2) the extra lithium intercalation sites created within the graphene sheets during the annealing process. A mechanism for carbon with a defected structure holding extra lithium ions has been proposed by Maier et al. [2]. In our case, using Fe₃O₄ nanorods/graphene nanocomposite incorporates the desirable characteristics of Fe₃O₄ nanorods and graphene sheets in the composite, and a strong synergistic effect is realized.

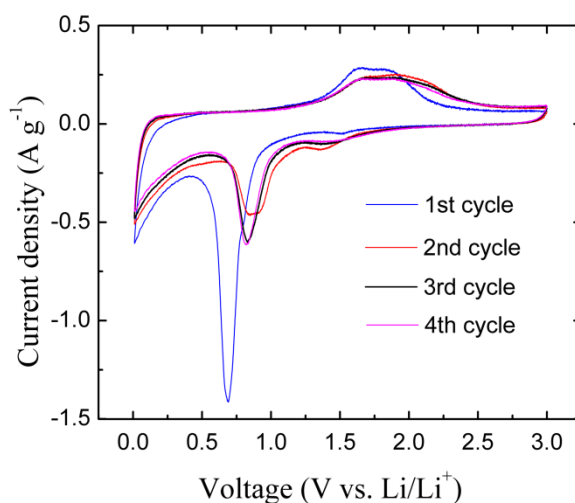
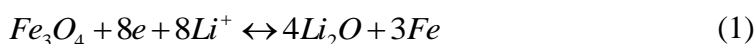


Figure 7. Initial four cycles of CV curves of Fe₃O₄/graphene electrodes.

Figure 7 presents the CV of the as-synthesized Fe₃O₄/graphene composite electrodes. During the first cycle, a cathodic peak at 0.65 V and a broad anodic peak at about 1.7 V are observed, which correspond to the reduction of Fe³⁺ ions and the reverse oxidation process. This result agrees well with the first discharge curve for the electrode synthesized from micro-sized Fe₃O₄. The formation of Fe and Li₂O and the re-formation of Fe₃O₄ can be described by the following electrochemical conversion reaction.



In the second cycle, the main reduction peak at 0.65 V is shifted to 0.83 V, probably due to the formation of solid electrolyte interface and realign of Fe₃O₄ nanorods. The intensity and integral areas for the third and fourth cycles are similar (Figure 7), which indicates that the electrochemical stability of the Fe₃O₄/graphene composite is reached quickly after a few initial cycles.

The rate capability of the $\text{Fe}_3\text{O}_4/\text{graphene}$ electrode was evaluated at various current densities, and the results are shown in Figure 8. For comparison, the rate performance of pure Fe_3O_4 and pure graphene electrodes also are shown in Figure 8. The $\text{Fe}_3\text{O}_4/\text{graphene}$ composite possesses a reversible capacity of 1200 mAh g^{-1} after five cycles at a current density of 100 mA g^{-1} , whereas the reversible capacity of Fe_3O_4 and graphene decreases to 323 mAh g^{-1} and 770 mAh g^{-1} respectively.

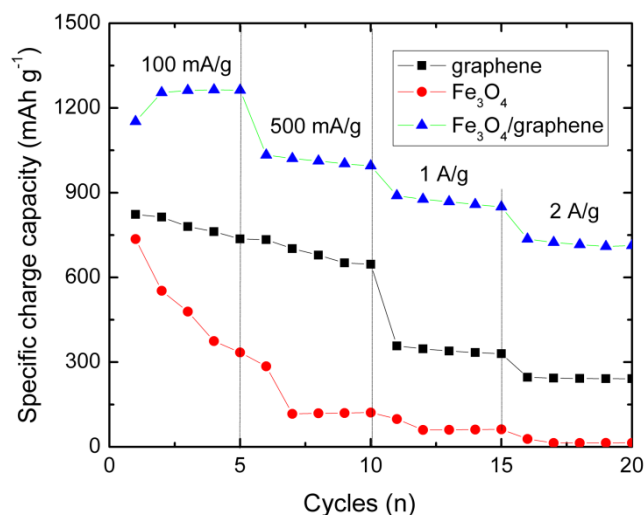


Figure 8. Rate capabilities of the $\text{Fe}_3\text{O}_4/\text{graphene}$ composite, micro-sized Fe_3O_4 , and graphene at various current densities. The applied current for discharge and charge process of each cycle is the same.

The charge capacity of the $\text{Fe}_3\text{O}_4/\text{graphene}$ composite decreases to and stabilizes at 1026 mAh g^{-1} , 871 mAh g^{-1} , and 721 mAh g^{-1} at a current density of 500 mA g^{-1} , 1000 mA g^{-1} and 2000 mA g^{-1} , respectively. It shows much better rate capability when compared with the pure graphene and Fe_3O_4 electrodes. For example, the capacity of $\text{Fe}_3\text{O}_4/\text{graphene}$ is about three times the capacity of graphene, while the capacity of Fe_3O_4 is only about 30 mAh g^{-1} at the current density of 1000 mA g^{-1} .

4. DISCUSSION

Comparing with previous reports on $\text{Fe}_3\text{O}_4/\text{carbon}$ based electrode materials, the $\text{Fe}_3\text{O}_4/\text{graphene}$ composite prepared by the two-step synthesis process exhibits a much higher reversible capacity (1200 mAh g^{-1} at a current density of 100 mA g^{-1}). For magnetite/carbon core-shell nanorod electrodes, Wexler et al. [12] reported a reversible capacity of 600 mAh g^{-1} , which decreased to about 400 mAh g^{-1} after 100 cycles. Guo et al. [17] synthesized Fe_3O_4 nanocrystals and a carbon composite that delivered a specific capacity of 600 mAh g^{-1} after about 30 cycles. Kim et al. [18] demonstrated that $\text{Fe}/\text{Fe}_3\text{O}_4$ core-shell nanostructure electrodes could have a reversible capacity of about 600 mAh g^{-1} after 50 cycles; however, because the iron is inactive during the intercalation process, the capacity is much lower than that of our $\text{Fe}_3\text{O}_4/\text{graphene}$ nanocomposite. Recently, Zhao et al. [41] synthesize the sandwich-structured graphene- Fe_3O_4 @carbon nanocomposites for lithium-ion

battery, which exhibits 960 mAh g^{-1} at a current density of 100 mA g^{-1} after 100 cycles. Zhu's group [42] prepared the hierarchical Fe_3O_4 microsphere/reduced graphene oxide composites as an anode for lithium-ion batteries, which exhibit 1100 mAh g^{-1} and 600 mAh g^{-1} at current densities of 100 mA g^{-1} and 1000 mA g^{-1} , respectively. Zuo et.al [43] reported the synthesis of carbon coated hollow Fe_3O_4 nanoparticles anchored on graphene with a particle size around 100nm. This composite have the reversible capacity of about 900 mAh g^{-1} and 745 mAh g^{-1} at current densities of 100 mA g^{-1} and 1000 mA g^{-1} , respectively. Table 1 exhibits a direct comparison on electrochemical properties with other works. It can be found that the obtained Fe_3O_4 /graphene structures show outstanding electrochemical performance. In our case, a higher reversible capacities of 1200 mAh g^{-1} and 720 mAh g^{-1} are obtained at 100 mA g^{-1} and 2000 mA g^{-1} , respectively. These results are similar to those obtained by single-wall nanotubes. We attribute the superior performance of our material to its higher surface area ($206 \text{ cm}^2/\text{g}$ comparing to $53 \text{ m}^2/\text{g}$), higher porosity ($1.105 \text{ cm}^3/\text{g}$ to $0.23 \text{ cm}^3/\text{g}$), and smaller diameter of the Fe_3O_4 nanorods. The high porosity ($1.105 \text{ cm}^3/\text{g}$) of the Fe_3O_4 /graphene nanocomposite and the flexibility of graphene sheets easily accommodate the volume expansions and contractions during lithium insertion and extraction, thus preventing aggregation of Fe_3O_4 nanorods and cracking or crumbling of the electrode material upon continuous cycling.

Table 1. Electrochemical properties of Fe_3O_4 /carbon based electrode materials

Electrode description	Current density (mA/g)	Specific capacity (mA h/g)	Reference
Fe_3O_4 nanoparticles/graphene	100	960	[41]
	1000	600	
Fe_3O_4 microsphere/graphene	100	1100	[42]
	1000	600	
Fe_3O_4 nanospheres/graphene	100	900	[43]
	1000	745	
Fe_3O_4 nanoflakes/graphene	100	1000	[44]
	1000	800	
Fe_3O_4 nanorods/graphene	100	800	[45]
	1000	650	
Fe_3O_4 @C quantum dots/graphene	200	800	[46]
	800	400	
This work	100	1200	
	1000	720	

The graphene sheets with homogeneously distributed nanoparticles serve as a good conductive media and, therefore, reduce the charge transfer resistance of the electrode. Furthermore, the high surface areas of the nanocomposite ($206 \text{ m}^2/\text{g}$) and the nanoscale diameters of Fe_3O_4 nanorods effectively increase the accessible sites and shorten the lithium ion transportation distances. All these factors contribute to the highly-reversible capacities and high rate capabilities observed in this work. The two-step synthesis approach used to synthesize the nanorod Fe_3O_4 /graphene composite also proved to be a facile approach for synthesizing this material for large scale applications.

5. CONCLUSIONS

A nanorod Fe_3O_4 material enhanced by a graphene nanocomposite was synthesized successfully using a two-step method. This material shows promise for use as an advanced anode material for high-energy, lithium-ion batteries. The Fe_3O_4 nanorods with diameters ranging from 50 nm to 100 nm are uniformly dispersed on and between the graphene sheets. This Fe_3O_4 /graphene composite has a high surface area and pore volume, which facilitate electrolyte penetration and accommodation of volume changes during the cycling process. Furthermore, the flexibility of graphene prevents the agglomeration of nanoparticles, and the nanoparticles, in turn, stop the restacking of graphene sheets. The good conductivity of graphene and the nanoscaled active material allow rapid electron transport and lithium-ion diffusion. Therefore, these Fe_3O_4 /graphene composite exhibits a high reversible capacity (1200 mAh g^{-1}), good cycle stability, and rate capability. These superior electrochemical performances demonstrate that the as-synthesized Fe_3O_4 /graphene composite is a promising candidate as an alternative anodes for high-performance lithium-ion batteries.

ACKNOWLEDGEMENTS

We acknowledge the financial supports by the National Natural Science Foundation of China (Nos. 51374255 and 51302323), Program for New Century Excellent Talents in University (NCET-13-0594), and Natural Science Foundation of Hunan Province, China (14JJ3018).

References

1. C. Liu, F. Li, L. P. Ma, H. M. Cheng, *Adv. Mater.*, 22 (2010) E28.
2. J. Ni, Y. Li, *Adv. Energy Mater.*, 6 (2016).
3. B. Luo, T. F. Qiu, D. L. Ye, L. Z. Wang, L. J. Zhi, *Nano Energy*, 22 (2016) 232.
4. J. Hassoun, G. Derrien, S. Panero, B. Scrosati, *Adv. Mater.*, 20 (2008) 3169.
5. L. F. Cui, Y. Yang, C. M. Hsu, Y. Cui, *Nano Lett.*, 9 (2009), 3370.
6. H. Hou, M. Jing, Y. Yang, Y. Zhu, L. Fang, W. Song, X. Ji, *ACS Appl. Mater. Interfaces*, 6 (2014) 16189.
7. S. J. Yang, S. Nam, T. Kim, J. H. Im, H. Jung, J. H. Kang, C. R. Park, *J. Am. Chem. Soc.*, 135 (2013) 7394.
8. Y. Wang, B. Wang, F. Xiao, Z. Huang, Y. Wang, C. Richardson, H. Yuan, *J. Power Sources*, 298 (2015) 203.
9. H. Hu, L. Yu, X. Gao, Z. Lin, X. W. Lou, *Energy Environ. Sci.*, 8 (2015) 1480.
10. P. Meduri, C. Pendyala, V. Kumar, G. U. Sumanasekera, M. K. Sunkara, *Nano Lett.*, 9 (2009) 612.

11. J.L.C. Rowsell, V. Pralong, L. F. Nazar, *J. Am. Chem. Soc.*, 123 (2001) 8598.
12. H. Liu, G. Wang, J. Wang, D. Wexler, *Electrochem. Commun.*, 10 (2008) 1879.
13. Q. Lin, J. Wang, Y. Zhong, J. Sunarso, M.O. Tade, L. Li, Z. Shao, *Electrochim. Acta*, 212 (2016) 179.
14. X. Wang, Y. Liu, H. Arandiyana, H. Yang, L. Bai, J. Mujtaba, H. Sun, *Appl. Surf. Sci.*, 389 (2016) 240.
15. J.M.D. Coey, A. E. Berkowitz, L. Balcells, F. F. Putris, F. T. Parker, *Appl. Phys. Lett.*, 72 (1998) 734.
16. W. M. Zhang, X. L. Wu, J. S. Hu, Y. G. Guo, L. J. Wan, *Adv. Funct. Mater.*, 18 (2008) 3941.
17. Z. M. Cui, L. Y. Hang, W. G. Song, Y. G. Guo, *Chem. Mater.*, 21 (2009) 1162.
18. G. H. Lee, J. G. Park, Y. M. Sung, K. Y. Chung, W. I. Cho, D. W. Kim, *Nanotechnology*, 20 (2009).
19. K. S. Novoselov, A. K. Geim, S.V. Morozov, D. Jiang, Y. Zhang, S. V. Dubonos, A. A. Firsov, *Science*, 306 (2004) 666.
20. A. H. Castro Neto, F. Guinea, N.M.R. Peres, K. S. Novoselov, A. K. Geim, *Rev. Mod. Phys.*, 81 (2009) 109.
21. F. Schedin, A. K. Geim, S. V. Morozov, E. W. Hill, P. Blake, M. I. Katsnelson, K. S. Novoselov, *Nat. Mater.*, 6 (2007) 652.
22. S. Z. Butler, S. M. Hollen, L. Cao, Y. Cui, J. A. Gupta, H. R. Gutierrez, J. E. Goldberger, *Acs Nano*, 7 (2013) 2898.
23. M. Zhi, C. Xiang, J. Li, M. Li, N. Wu, *Nanoscale*, 5 (2013) 72.
24. V. Georgakilas, M. Otyepka, A. B. Bourlinos, V. Chandra, N. Kim, K. C. Kemp, K. S. Kim, *Chem. Rev.*, 112 (2012) 6156.
25. G. Wang, X. Shen, J. Yao, J. Park, *Carbon*, 47 (2009) 2049.
26. E. Yoo, J. Kim, E. Hosono, H. S. Zhou, T. Kudo, I. Honma, *Nano Lett.*, 8 (2008) 2277.
27. Y. Zhao, C. Ma, Y. Li, H. Chen, Z. Shao, *Carbon*, 95 (2015) 494.
28. D. Chao, C. Zhu, X. Xia, J. Liu, X. Zhang, J. Wang, H. J. Fan, *Nano Lett.*, 15 (2015) 565.
29. M. Yu, A. Wang, Y. Wang, C. Li, G. Shi, *Nanoscale*, 6 (2014) 11419.
30. A. Bhaskar, M. Deepa, M. Ramakrishna, T. N. Rao, *J. Phys. Chem. C*, 118 (2014) 7296.
31. B. Zhao, T. Wang, L. Jiang, K. Zhang, M.M.F. Yuen, J. B. Xu, C. P. Wong, *Electrochim. Acta*, 192 (2016) 205.
32. G. Zhou, D. W. Wang, F. Li, L. Zhang, N. Li, Z. S. Wu, H. M. Cheng, *Chem. Mater.*, 22 (2010) 5306.
33. C. Ban, Z. Wu, D. T. Gillaspie, L. Chen, Y. Yan, J. L. Blackburn, A. C. Dillon, *Adv. Mater.*, 22 (2010) E145.
34. S. Stankovich, D. A. Dikin, G.H.B. Dommett, K. M. Kohlhaas, E. J. Zimney, E. A. Stach, R. S. Ruoff, *Nature*, 442 (2006) 282.
35. K. N. Kudin, B. Ozbas, H. C. Schniepp, R. K. Prud'homme, I. A. Aksay, R. Car, *Nano Lett.*, 8 (2008) 36.
36. A. Pan, D. Liu, X. Zhou, B. B. Garcia, S. Liang, J. Liu, G. Cao, *J. Power Sources*, 195 (2010) 3893.
37. D. Liu, B. B. Garcia, Q. Zhang, Q. Guo, Y. Zhang, S. Sepehri, G. Cao, *Adv. Funct. Mater.*, 19 (2009) 1015.
38. D. W. Wang, F. Li, M. Liu, G. Q. Lu, H. M. Cheng, *Angew. Chem., Int. Ed.*, 47 (2008) 373.
39. S. Yang, G. Cui, S. Pang, Q. Cao, U. Kolb, X. Feng, K. Mullen, *ChemSuschem*, 3 (2010) 236.
40. P. Guo, H. Song, X. Chen, *Electrochem. Commun.*, 11 (2009) 1320.
41. L. Zhao, M. Gao, W. Yue, Y. Jiang, Y. Wang, Y. Ren, F. Hu, *ACS Appl. Mater. Interfaces*, 7 (2015) 9709.
42. K. Zhu, Y. Zhang, H. Qiu, Y. Meng, Y. Gao, X. Meng, Y. Wei, *J. Alloys Compd.*, 675 (2016) 399.

43. Y. Zuo, G. Wang, J. Peng, G. Li, Y. Ma, F. Yu, C. P. Wong, *J. Mater. Chem. A*, 4 (2016) 2453.
44. B. Zhao, Y. Zheng, F. Ye, X. Deng, X. Xu, M. Liu, Z. Shao, *ACS Appl. Mater. Interfaces*, 7 (2015) 14446.
45. J. Jiao, W. Qiu, J. Tang, L. Chen, L. Jing, *Nano Res.*, 9 (2016) 1256.
46. S. Zhao, D. Xie, X. Yu, Q. Su, J. Zhang, G. Du, *Mater. Lett.*, 142 (2015) 287.

© 2017 The Authors. Published by ESG (www.electrochemsci.org). This article is an open access article distributed under the terms and conditions of the Creative Commons Attribution license (<http://creativecommons.org/licenses/by/4.0/>).